# Intramolecular Hydrogen Bonding in 2-Chloroethanol and 2-Bromoethanol and Anisotropic Interactions with He*($2^3$S) Metastable Atoms: Two-Dimensional Penning Ionization Electron Spectroscopy Combined with Quantum Chemistry Calculations

**Shan Xi Tian, Naoki Kishimoto, and Koichi Ohno***

*Department of Chemistry, Graduate School of Science, Tohoku University, Aramaki, Aoba-ku, Sendai 980-8578, Japan*

*Received: August 22, 2002*

Five stable isomers of 2-chloroethanol and 2-bromoethanol have been found by the density functional theory with the hybrid density-functional B3LYP and the second-order Møller−Plesset perturbation method using 6-31++G(d,p) and 6-311++G(2d,2p) basis sets. Intramolecular hydrogen bonding plays an important role in the most stable isomers. Assignments, especially for the low ionization potential bands, in the He*($2^3$S) Penning ionization electron spectra and He I ultraviolet photoelectron spectra were made on the basis of the characteristics of molecular orbitals, collision energy dependence of partial Penning ionization cross sections (CEDPICS), and the related calculations. The intramolecular hydrogen bonding (C−Cl···H−O and C−Br···H−O) leads to the significant steric shielding effects, which further results in distinctly different slopes of CEDPICS for the low ionization potential bands.

## I. Introduction

Two-dimensional (electron-energy and collision-energy-resolved) Penning ionization electron spectroscopy (2D-PIES) has been used effectively to investigate anisotropic interactions around the target molecules (M).[1−7] Steric anisotropy reflected in the Penning ionization process ($A^* + M \rightarrow M^+ + A + e^-$) is theoretically based on the electron exchange model[8] and spatial electron distribution of molecular orbitals (MO).[9] The former suggests the facts that an electron of an MO of the target M is transferred to the inner-shell orbital of a metastable atom A*, and the excited electron of A* is ejected as the Penning electron $e^-$. Obviously, transition probability to each ionic state in Penning ionization is governed by an overlap of the related orbitals. On the other hand, the spatial electron distributions of an MO are usually localized at certain parts of the molecular skeleton. Thereby, for a given A* (e.g., a He*($2^3$S) metastable atom), band intensities in a Penning ionization electron spectrum (PIES) are closely related to the MO electron density distributions. Furthermore, the characteristics of spatial distributions of MOs and the related anisotropic interactions with He*($2^3$S) atoms can be studied by measurements of collision energy ($E_c$) dependence of partial ionization cross sections (CEDPICS)[1,2,10] and collision-energy-resolved PIES (CERPIES).[1,2,11] Typically, CEDPICS exhibits a positive slope for a repulsive interaction; namely the partial ionization cross sections are enhanced at the higher $E_c$ values because a faster He* atom can reach the reactive region effectively. On the contrary, if an attractive interaction governs the ionization reaction, the partial cross sections decrease with increasing $E_c$ values, CEDPICS accordingly shows a negative slope. Moreover, peak shifts ($\Delta E$) in a PIES with respect to He I ultraviolet photoelectron spectrum (UPS) supply us with information on the entrance channel of the Penning ionization process. A large negative shift indicates that there is an attractive potential well on the interaction potential energy curve. A positive one indicates that there is a strong repulsive wall. The slope parameters ($m$) of CEDPICS together with $\Delta E$ values can give us the details of the anisotropic potential surface around the target molecule. In our laboratory, CEDPICS can be obtained by simultaneously measuring CERPIES using the 2D-PIES technique. 2D-PIES studies of some polyatomic molecules (from small diatomic molecules such as $N_2$[3] and CO[4] to the bigger hydrocarbons such as anthracene[5] and adamantane[6]) by collision with the He* ($2^3$S) atoms have been reported so far. Among these studies, nonbonding lone pair orbitals ($n$) attract particular interest because they play an essential role in hydrogen bonding (HB), which is a hot topic of current spectroscopic investigations.[12]

It is noted that variations in reactivity of $n$ electrons due to intramolecular HB have been observed in PIES by Ohno et al. for $XCH_2CH_2OH$ (X = Cl, Br, $NH_2$, and $N(CH_3)_2$).[13] The authors suggested that the intramoelcular HB in 2-chloroethanol ($ClCH_2CH_2OH$) resulted in a significant steric shielding effect by observing the different intensities of the $n_{Cl}$ bands in PIES.[13] In the He*($2^3$S) PIES, these split bands usually show different intensities that may be interpreted by their different spin states. The PIES measured by Ohno et al. were the collision-energy averaged spectra using the metastable He*($2^3$S) atoms produced by electron impacts.[13] They are remeasured in this work by a discharged source in the thermal energy range.[10] Furthermore, it is worth performing 2D-PIES experiments on both 2-chloroethanol and 2-bromoethanol ($BrCH_2CH_2OH$) to get insight into the steric shielding effects arising from the intramolecular HB.

For reasonable assignments in the PIES and UPS, we need to locate the stable isomers of $ClCH_2CH_2OH$ and $BrCH_2CH_2OH$ by searching their molecular potential surfaces. It is well-known that the $YCH_2CH_2X$ (X, Y = halogen atoms, OH, $NH_2$, etc.) type molecules have floppy molecular potential surfaces because there are not only possible intramolecular HBs but also the translational and rotational mobility of the X and Y groups. To our best knowledge, there are no theoretical reports on the isomers of these two molecules until now. The density-functional theory (DFT) with the Becke's three-parameter and Lee−Yang−

10.1021/jp021941w CCC: $25.00 
Published on Web 12/06/2002

Parr hybrid functional (B3LYP)[14] and the second-order Møller−Plesset perturbation (MP2) method[15] with 6-31++G(d,p) and 6-311++G(2d,2p) basis sets are employed for the calculations of the isomeric systems in this work.

## II. Experimental Section

Details of the experimental apparatus have been reported elsewhere.[1,2,10] Metastable atoms of He*($2^1$S, $2^3$S) were produced by a discharged nozzle source with a tantalum hollow cathode. The He*($2^1$S) component was quenched by a water-cooled helium discharge lamp. He I resonance photons (584 Å, 21.22 eV) produced by a discharge in pure helium gas were used to obtain UPS. The kinetic energies of the electrons ejected in Penning ionization or photoionization were determined by a hemispherical electrostatic deflection type analyzer using an electron collection angle 90° to the incident He*($2^3$S) beam axis or He I light beam axis. The energy resolution of the electron analyzer was estimated to be 80 meV from the full width at half-maximum (fwhm) of the $Ar^+(^2P_{3/2})$ peak in the He I UPS for the energy higher resolution PIES and UPS measurements of the samples; for the CEDPICS measurements, the resolution was lowered to 250 meV to obtain higher electron counting rates. The transmission efficiency curves of the electron energy analyzer for both of these two modes were determined by comparing our UPS data of some molecules with those obtained by Gardner and Samson[16] and Kimura et al.[17] The calibration of the electron energy scale was made with reference to the lowest ionic state of molecule nitrogen mixed with the sample molecule in He I UPS ($E_e$ = 5.639 eV)[18] and He*($2^3$S) PIES ($E_e$ = 4.292 eV)[19] including a peak energy shift of 50 meV and the difference between the metastable excitation energy and the lowest ionization potential (IP).

For the collision-energy-resolved measurements of Penning ionization, the metastable He*($2^3$S) beam was modulated by a pseudorandom chopper rotating at ca. 400 Hz and then introduced into a reaction cell located at 504 mm downstream from the chopper disk. Time dependent electron signals for each kinetic electron energy $E_e$ were recorded with scanning electron energies of a 40 meV step and the dwell time for the TOF measurements was 3 $\mu$s. The two-dimensional data as functions of $E_e$ and time $t$ were stored in a 2 MB RAM. Two-dimensional spectra $I_e(E_e,t_{TOF})$, functions of $E_e$ and TOF, can lead to $I_e(E_e,v_{He^*})$, functions of $E_e$ and the velocity of He* ($v_{He^*}$), and then to the two-dimensional Penning ionization cross-section $\sigma(E_e,v_r)$ using the equations,

$$\sigma(E_e,v_r) = c\{I_e(E_e,v_{He^*})/I_{He^*}(v_{He^*})\}(v_{He^*}/v_r) \quad (1)$$

$$v_r = [{v_{He^*}}^2 + 3kT/M]^{1/2} \quad (2)$$

where $c$ is a constant, $v_r$ is the relative velocity averaged over the velocity of the target molecule, $k$ is the Boltzmann constant, and $T$ and $M$ are the gas temperature and mass of the target molecule, respectively. The velocity distribution $I_{He^*}(v_{He^*})$ of the He* beam was determined by monitoring secondary electrons emitted from the inserted stainless steel plate. Finally, $\sigma(E_e,v_r)$ was normalized by $I_{He^*}(v_{He^*})$ and converted to $\sigma(E_e,E_c)$, functions of $E_e$ and $E_c$, using the relation

$$E_c = \mu {v_r}^2/2 \quad (3)$$

where $\mu$ is the reduced mass of the system. The CEDPICS were obtained from $\sigma(E_e,E_c)$ data within an appropriate range of $E_e$ (typically the fwhm of the respective band) to avoid the effect of neighboring bands. The CERPIES were cut at the two $E_c$ (lower and higher) values from $\sigma(E_e,E_c)$ data with some width. To study the low-ionization-potential bands, we measured the CERPIES in the ranges of $E_e$: 7.5−9.5 eV for $ClCH_2CH_2OH$ and $E_e$: 7.5−9.75 eV for $BrCH_2CH_2OH$ at the high energy resolution condition.

2-Chloroethanol (99%) and 2-bromoethanol (99%) were purchased from Wako Pure Chemical Industries Ltd. They were used after several freeze−pump−thaw cycles. The liquid sample was contained in a Pyrex tube out of the chamber in the experiments, the Pyrex tube was connected with a steel tube inserted into the reaction cell in the chamber. The volatility of the samples at room temperature was high enough to create a sufficient concentration of target molecules in the gas phase, the ambient pressure was controlled at ca. $2 \times 10^{-5}$ Torr.

## III. Calculation Methods

According to the OH orientations, the isomers can be classified to two types, gauche (G) and stagger (A). All of the possible isomers were optimized then their stabilities were checked by the harmonic frequency calculations at the DFT-B3LYP and MP2 levels with the 6-31++G(d,p) basis set. We calculated the relative total electron energies without ($E_{tot}$) and with zero point vibration energy (ZPVE) corrections ($E_{tot}^{ZPVE}$) among the stable isomers. Composition ratio ($\rho$) for each isomer of $ClCH_2CH_2OH$ or $BrCH_2CH_2OH$ was estimated by an exponent function,

$$\rho \propto \exp\left(\frac{\Delta E_{tot}^{ZPVE}}{kT}\right) \quad (4)$$

The geometrical parameters of the most stable isomers were re-optimized with the 6-311++G(2d,2p) basis set. This split valence basis set argued with the double d polarization functions to the heavy atoms and the double p polarization functions to the H atoms is frequently used for studying HB clusters, and its reliability has been proved.[20] Hartree−Fock self-consistent-field (HF−SCF) calculations with the 6-311+G(2d,2p) basis set were performed for drawing electron density maps of respective MO; thick solid curves indicate the repulsive molecular surface approximated by atomic spheres of van der Waals radii.[21] The IP values were also calculated for assignments in the He I UPS and PIES by outer valence Green's function (OVGF) method[22,23] with the 6-31+G(d) basis set.

It is well-known that the shape of velocity dependence of the total scattering cross section of He*($2^3$S) by He, Ar, and Kr is very similar to that of Li($2^2$S),[24] and interaction well depths and location of potential wells have been found to be very similar for interactions of various targets with He*($2^3$S) and Li($2^2$S).[25] For atomic targets (H, Li, Na, K, and Hg), quantitative estimation of the well depth was summarized to be in good agreement with the ratio of 1.1 and 1.2 by the Li model potential with respect to He*($2^3$S) in a recent study.[26] So this similarity between He*($2^3$S) and Li($2^2$S) is usually used to compare the computationally much more feasible Li−M potentials with the experimental results on the He*($2^3$S)−M interactions.[2−7] In this study, the interaction potential calculations with the Li($2^2$S) atom, $V^*(R,\theta)$ (where $R$ and $\theta$ were defined in the figures), were performed at the unrestricted MP2 level of theory using the 6-31+G(d,p) basis set with scanning $R$ or $\theta$ values and the geometrical parameters of the targets fixed at the previously optimized values. Spin contamination is negligible for these

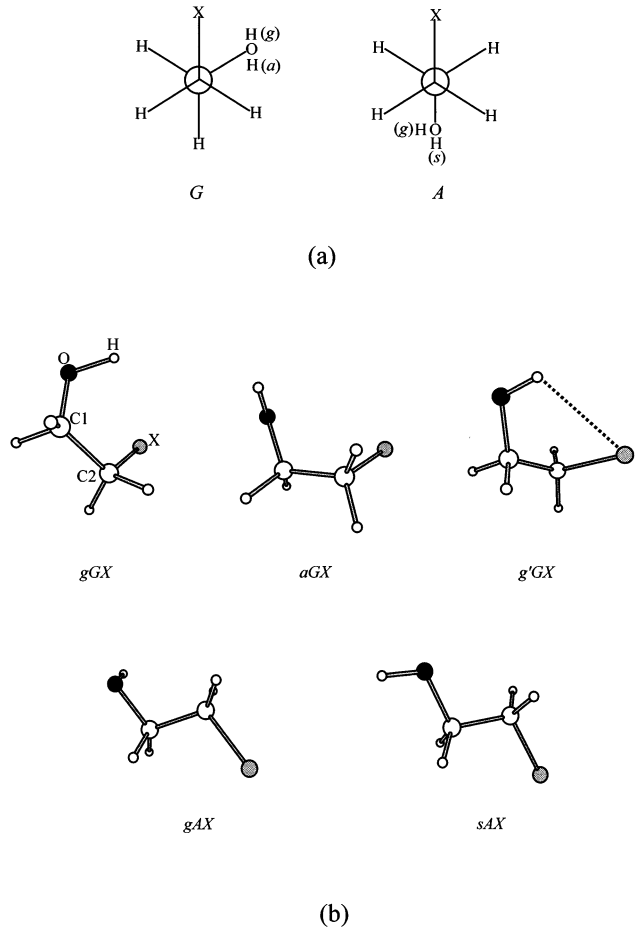


**Figure 1.** (a) Newman projections of 2-halogenoethanol (here X = Cl or Br). (b) Isomeric conformers (the geometrical parameters are optimized at the DFT-B3LYP/6-31++G(d,p) level).

calculations. The present calculations of interaction potentials and IP values were performed with GAUSSIAN 98.[27]

## IV. Results and Discussions

**A. Results.** Newman projections of the stable isomers are shown in in Figure 1a, and their structures determined at the DFT-B3LYP/6-31++G(d,p) level are shown in Figure 1b. It is noted that only sAX is of $C_s$ symmetry whereas the others flee from the $C_s$ symmetry geometry, and the intramolecular HB occurs in g′GX conformer. The optimizations of aGBr were always converged to the geometry of gGBr at the MP2 level of theory using the smaller 6-31++G(d,p) and bigger 6-311++G(2d,2p) basis sets.

The He I UPS and He*($2^3$S) PIES of $ClCH_2CH_2OH$ and $BrCH_2CH_2OH$ are shown in Figures 2 and 3, respectively. The energy scale for PIES is shifted 1.40 eV relative to that for UPS by the difference in the excitation energies between the He I photon (21.22 eV) and the He*($2^3$S) (19.82 eV).

Parts a and b of Figure 4 show the CERPIES of $ClCH_2CH_2OH$ and $BrCH_2CH_2OH$, respectively. In Figure 4a, the hot spectrum at the higher $E_c$ ca. 250 meV (238−262 meV) is exhibited by the dotted curve, and the cold spectrum at the lower $E_c$ ca. 105 meV (102−108 meV) is exhibited by the solid curve. In Figure 4b, the hot spectrum at the higher $E_c$ ca. 250 meV (239−261 meV) is exhibited by the dotted curve, and the cold spectrum at the lower $E_c$ ca. 100 meV (95−105 meV) is exhibited by the solid curve.

log $\sigma$ vs log $E_c$ plots of CEDPICS in a collision energy range 90−300 meV are exhibited in Figures 5 and 6 for $ClCH_2CH_2OH$ and $BrCH_2CH_2OH$, respectively. Electron density maps plotted on *XY* plane of the most stable isomer are also shown in the figures for grasping effective access directions of the He* atoms. Due to the low $C_1$ symmetry of the conformer, the schematic diagrams of the MOs are presented together with the density maps for easily recognizing the MO characteristics, where the solid circles represent valence s orbital, and couples of ellipses and dashed circles represent in-plane and out-of-plane components of p orbitals.

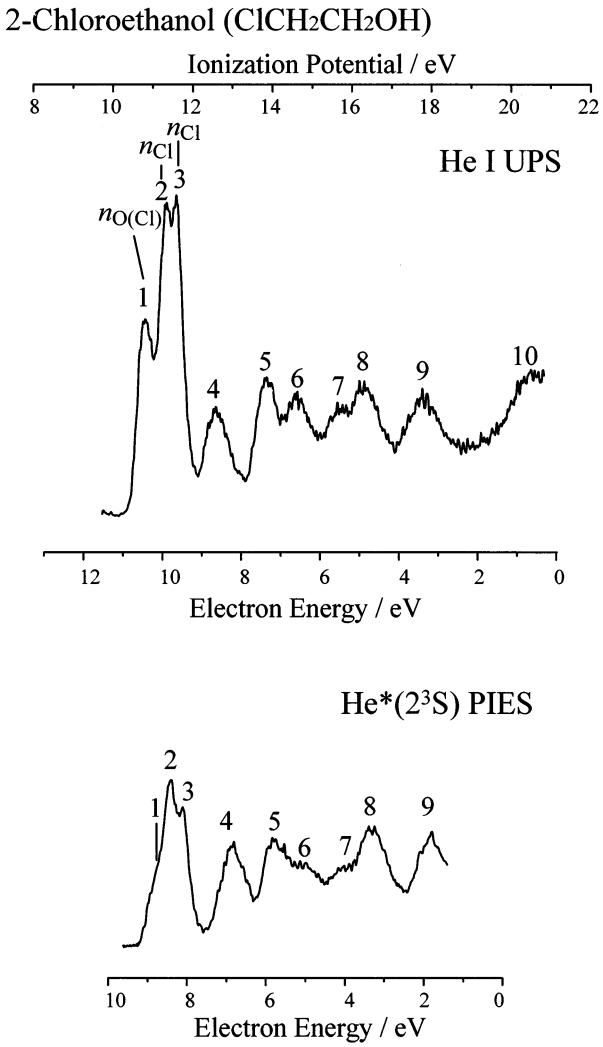


**Figure 2.** He I UPS and He*($2^3$S) PIES of 2-chloroethanol ($ClCH_2CH_2OH$).

Figures 7 and 8 show the CERPIES and CEDPICS measured at the high energy resolution condition for bands 1−3. In Figure 7a, the cold spectrum ($E_c$: 116−124 meV, averaged 120 meV) is exhibited by the solid curve, whereas the hot spectrum ($E_c$: 238−262 meV, averaged 250 meV) is exhibited by the dotted curve. In Figure 8a, the cold spectrum ($E_c$: 92−98 meV, averaged 95 meV) is exhibited by the solid curve, whereas the hot spectrum ($E_c$: 263−277 meV, averaged 270 meV) is exhibited by the dotted curve. In Figures 7b and 8b, the plots of the three highest occupied MO are plotted with MOLDEN,[28] where the contours for the most stable isomer represent amplitudes of ±0.01. The arrows represent the attractive interactions, whereas the broken curves represent the repulsive interactions.

The model interaction Li−M potentials $V^*(\theta,R)$ are shown in Figures 9 and 10. The details can be read in the captions. These figures are used to capture the general characteristics of

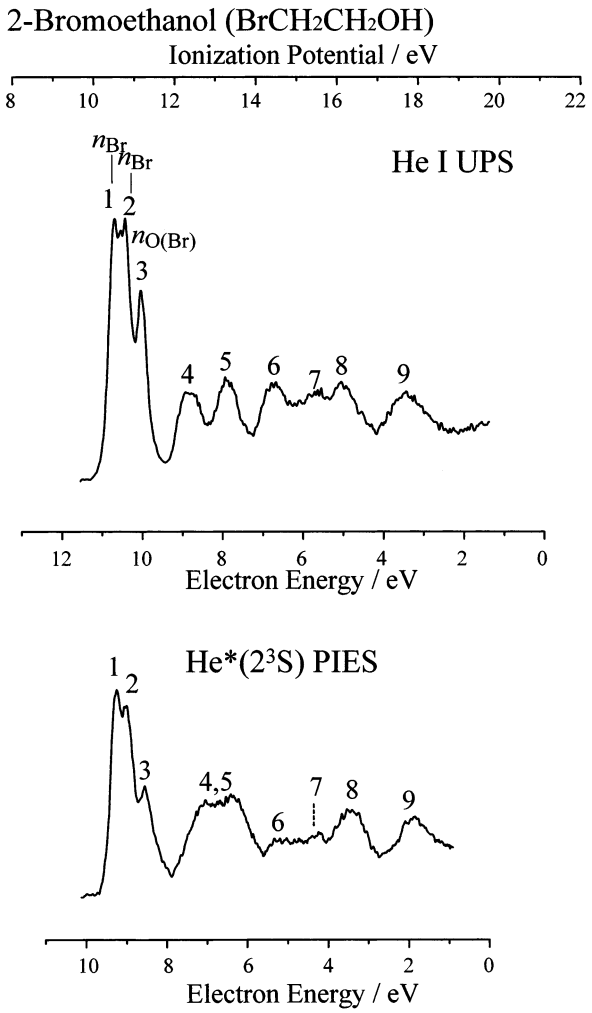


**Figure 3.** He I UPS and He*($2^3$S) PIES of 2-bromoethanol ($BrCH_2CH_2OH$).

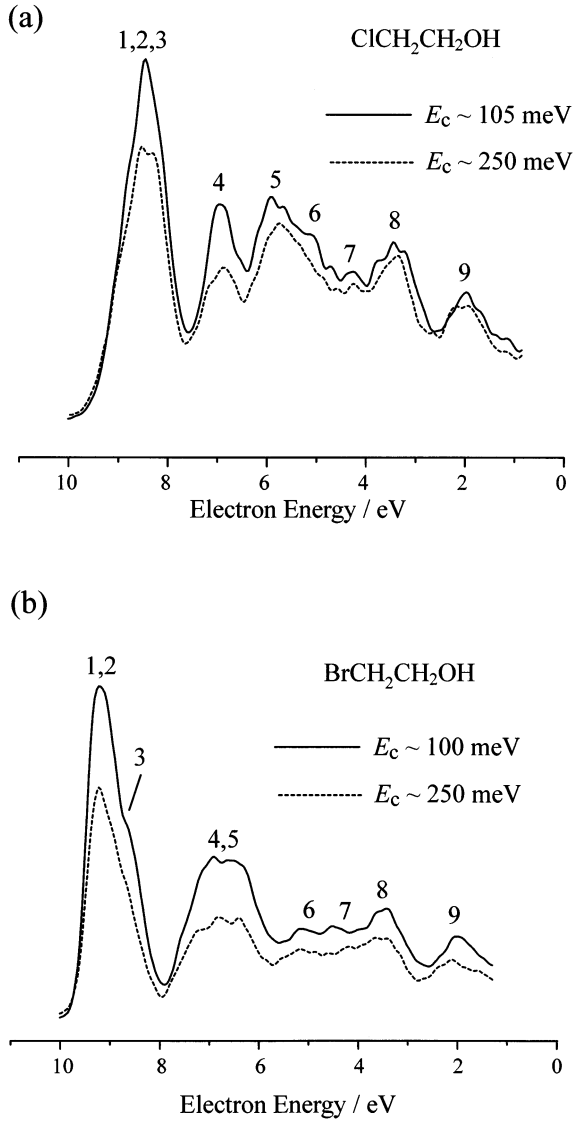


**Figure 4.** (a) Collision-energy-resolved He*($2^3$S) PIES of $ClCH_2CH_2OH$: solid curve, $E_c \sim 102-108$ meV, average 105 meV; dotted curve, $E_c \sim 238-262$ meV, average 250 meV. (b) Collision-energy-resolved He*($2^3$S) PIES of $BrCH_2CH_2OH$: solid curve, $E_c \sim 95-105$ meV, average 100 meV; dotted curve, $E_c \sim 239-261$ meV, average 250 meV.

the anisotropic interactions and the differences of the interactions around the Cl and Br atoms.

Table 1 lists $\delta E_{tot}$, $\delta E_{tot}^{ZPVE}$, and the normalized composition ratios estimated with eq 4. The geometrical parameters and dipole moments of the most stable isomer, g′GX (X = Cl, Br), optimized at the DFT-B3LYP and MP2 levels with the 6-311++G(2d,2p) basis sets are summarized in Table 2. In Table 3, the three lowest IPs for four most stable isomers of each molecule were predicted with the OVGF calculations and at Koopmans' approximation using HF and B3LYP orbital energies. The experimental IP values obtained in this work and cited from the previous work[13] are also listed for comparison. The main orbital characteristics are given for each band.

Tables 4 and 5 summarize the experimental IPs and the calculated values for the most stable g′GX, experimental peak shifts $\Delta E$, slope parameters ($m$) of CEDPICS, and the band assignments with the orbital characteristics. The slope parameters were obtained by a least-squares fitting of the log $\sigma$ vs log $E_c$ plots. The vertical IPs were determined from present He I UPS. The $\Delta E$ values were obtained as the differences between the peak positions in PIES ($E_{PIES}$, in electron energy scale) and the nominal value ($E_0$, difference between the metastable excitation energy and sample IP), $\Delta E = E_{PIES} - E_0$.

**B. Isomers and Intramolecular Hydrogen Bonding.** The conformations of 2-halogenoethanols would be governed by three factors: (a) electrostatic interaction because of mutual repulsion of C−X and C−O dipoles, (b) hindered rotation around the C−C bond, and (c) stabilization resulting from the intramolecular HB.[29] The former two lead to the staggered conformers being more stable than the gauche ones (except for g′GX), which is in good agreement with the calculated results in Table 1. However, the g′GX conformer is the most stable because of the intramolecular HB. The frequency shifts of the OH stretching mode have been observed for 2-halogenoethanols.[29,30] The intramolecular HB energies in 2-halogenoethanols can be crudely estimated by comparison of relative stability between gGX or aGX and g′GX. Kolbjon and Hedberg reported the energy difference to be ca. 10 kJ/mol for 2-chloroethanol from electron diffraction data in the gas phase.[31] This value is close to our calculations (7.76−11.43 kJ/mol). Furthermore, this value for 2-bromoethanol should be a little larger than that for 2-chloroethanol on the basis of the calculated results in Table 1. The ratios estimated with eq 4 indicate that g′GX predominates at room temperature. The other isomers cannot be reflected in the spectra in this work due to low-energy resolution and broad ionization bands including vibration structures. Therefore, we subsequently analyze the geometrical parameters of g′GX in detail.

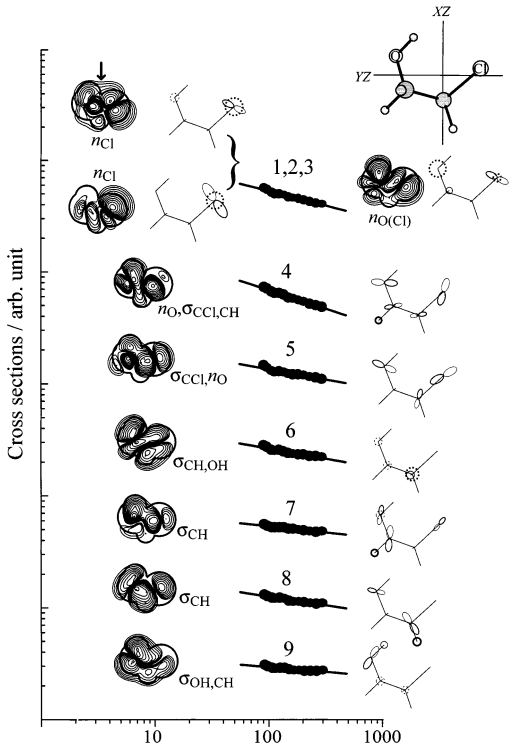


**Figure 5.** Collision energy dependence of partial ionization cross sections for $ClCH_2CH_2OH$ collided by He*($2^3S$). The density maps of the MOs of the most stable isomer are plotted on the plane *XY*. The black arrow points to the overlap density arising from the intramolecular hydrogen bonding OH···Cl.

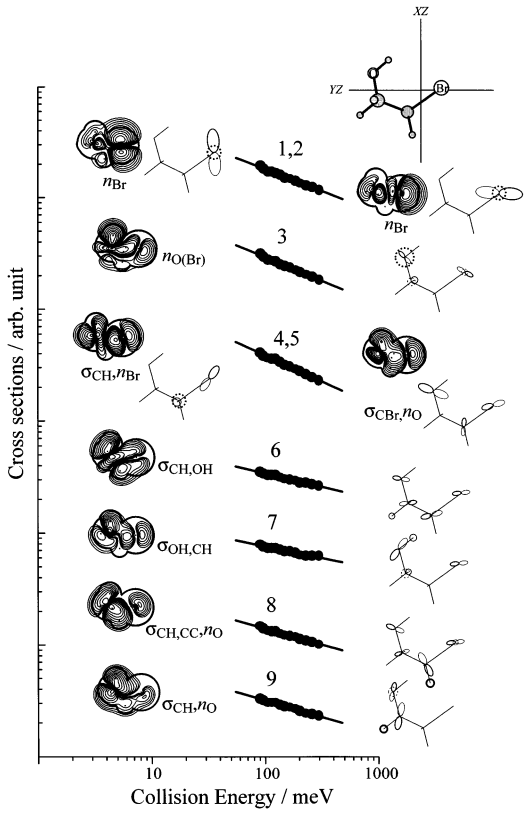


**Figure 6.** Collision energy dependence of partial ionization cross sections for $BrCH_2CH_2OH$ collided by He*($2^3S$). The density maps of the MOs of the most stable isomer are plotted on the plane *XY*.

As shown in Table 2, the results calculated by the DFT-B3LYP method differ from those obtained by the MP2 method.

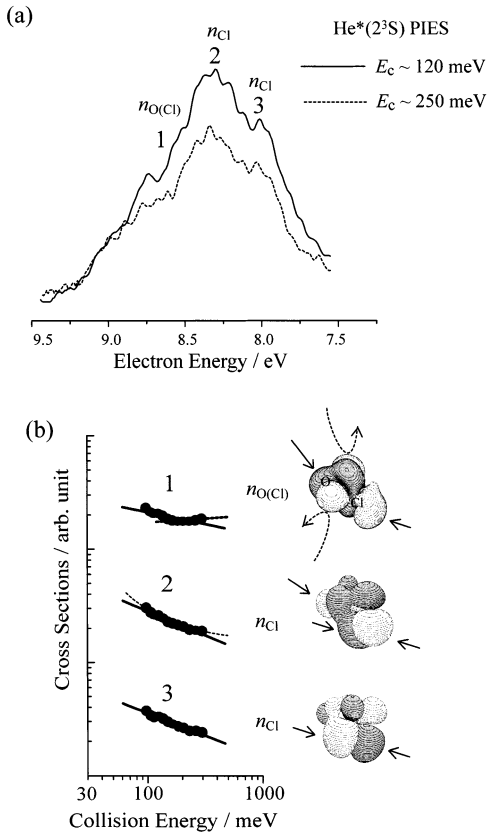


**Figure 7.** (a) Collision-energy-resolved He*($2^3S$) PIES of $ClCH_2CH_2OH$ measured at the high energy resolution condition: solid curve, $E_c$ ~ 116−124 meV, average 120 meV; dotted curve, $E_c$ ~ 238−262 meV, average 250 meV. (b) Collision energy dependence of partial ionization cross sections of bands 1−3 for $ClCH_2CH_2OH$ collided by He*($2^3S$). The contours for the most stable isomer represented amplitudes of ±0.01. The molecular geometry is enlarged for recognizing the MO characteristics.

In particular, the value of the HB length for each molecule predicted by the MP2 method is smaller by ca. 0.08 Å than that predicted by the DFT-B3LYP method. The MP2 value of the dihedral angle D(ClC2C1O) being smaller than the DFT-B3LYP value and the MP2 value of the dihedral angle D(HOC2Cl) being larger than the DFT-B3LYP value indicate that the MP2 method predicted the dipole interaction between C−X and C−O to be relatively weak; namely, the intramolecular HB predicted by the MP2 method is stronger than that predicted by the DFT-B3LYP method for these two molecules. According to classifications of HB strength by the HB lengths,[12] the intramolecular HB in these two molecules is a weak one. However, it is noted that both DFT-B3LYP and MP2 methods predicted the intramolecular HB in $ClCH_2CH_2OH$ to be a little stronger than that in $BrCH_2CH_2OH$ because the HB length $r$(H···Cl) is shorter than $r$(H···Br). These results can be interpreted by the smaller electron affinity (EA) of Br atom ($EA_{Cl}$ = 1.81 eV, $EA_{Br}$ = 1.69 eV)[32] and stronger electrostatic repulsive interaction between Br and O atoms.

**C. Spectral Assignments, CEDPICS, and Anisotropic Interactions.** Kimura et al. assigned the low-ionization-potential bands in the spectra of $ClCH_2CH_2OH$ to $n_{Cl}$, $n_{Cl}$, and $n_O$ on the basis of the SCF MO characteristics.[17] However, Ohno et al. gave a different sequence, $n_O$, $n_{Cl}$, and $n_{Cl}$, which was supported by three factors:[13] (a) the calculated splitting for the two $n_{Cl}$ orbitals was 0.16 eV, which was in good agreement with the observed separation between bands 2 and 3 (11.71−11.48 = 0.23 eV) and much larger than the corresponding values for

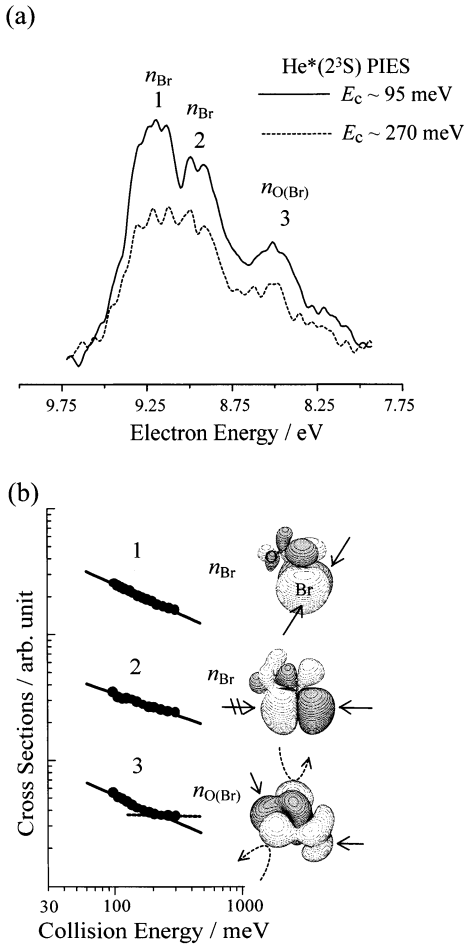


**Figure 8.** (a) Collision-energy-resolved He*($2^3$S) PIES of $BrCH_2CH_2OH$ measured at the high energy resolution condition: solid curve, $E_c$ ~ 92−98 meV, average 95 meV; dotted curve, $E_c$ ~ 263−277 meV, average 270 meV. (b) Collision energy dependence of partial ionization cross sections of bands 1−3 for $BrCH_2CH_2OH$ collided by He*($2^3$S). The contours for the most stable isomer represent amplitudes of ±0.01. The molecular geometry is enlarged for recognizing the MO characteristics.

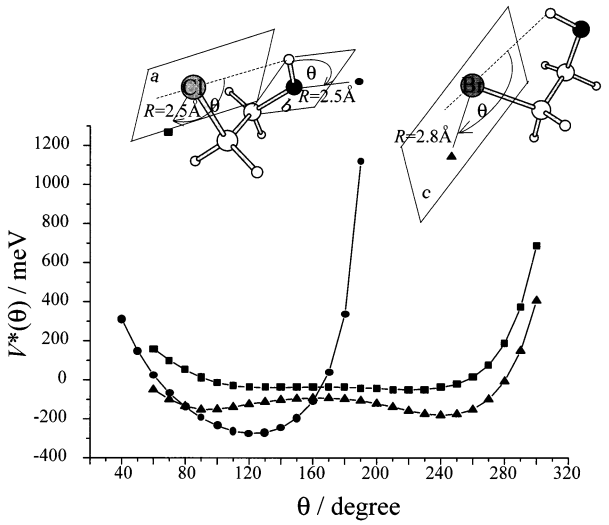


**Figure 9.** Interaction potential energy curves $V^*(\theta)$: ■, scanning $\theta$ around the Cl atom on the plane a which is perpendicular to C−Cl bond axis; ●, scanning $\theta$ around the O atom on the plane b (the HOC plane); ▲, scanning $\theta$ around the Br atom on the plane c which is perpendicular to C−Br bond axis. The distances between Li and Cl, O, or Br are shown in the figure.

bands 1 and 2 (11.48−10.91 = 0.57 eV); (b) the band shape for the $n_O$ orbital was rather broad in both UPS and PIES in comparison with the case for $n_{Cl}$ orbital; (c) it was based on the propensity found in the PIES for $CH_3CH_2X$ (X = OH, Cl, $NH_2$, etc.). In this work, we supply further proof supporting the assignments given by Ohno et al., owing to the developments of experimental and computational techniques.

In Table 3, the calculated IPs for the stable isomers are listed together with the experimental values. The discrepancies between the experimental IPs obtained in this work and those in the previous work[17] may be due to the electron energy calibrations for the spectra. However, the splitting energies among the bands observed in this work are close to the values observed previously.[17] The orbital characteristics are determined by the calculated MO wave functions. It is interesting that the band (orbital) sequences for the $ClCH_2CH_2OH$ isomers predicted by the DFT-B3LYP method differ distinctly from those predicted by the HF method. The sequences by the HF method are the same as those by the OVGF calculations. It can be explained by the following facts: the electron correlation effect included in the B3LYP functional should be important to predict a correct electron configuration although this method gives much smaller orbital energies, and a too crude approximations may be used in the OVGF method encoded in the GAUSSIAN program for highly efficient computations. For the latter, the OVGF method can be considered as a quasiparticle approximation of the electron propagator theory.[23] Using the HF wave functions, the third-order perturbation[23] (used for predicting the IPs in Tables 3−5) is still not powerful enough to predict the correct final states for this case. However, the band splitting energy predicted by the OVGF method, 0.26 eV between bands 2 and 3, is extremely close to the observed value (11.50−11.27 = 0.23 eV). Moreover, the IPs of the bands for $BrCH_2CH_2OH$ predicted by the OVGF method are in good agreement with the observed values (see Table 5).

Because of the $C_1$ molecular symmetry and intramolecular orbital ($n_X \leftrightarrow n_O$) interactions, the electron distributions of respective MO are delocalized. Thereby, the $n_O$ bands in the previous work are replaced by the $n_{O(Cl)}$ or $n_{O(Br)}$ in the assignments. The spectral assignments in this work are not only based on the facts presented by Ohno et al.[13] but also supported by subsequent discussions. We describe briefly the anisotropic interactions with the He* atoms around these two molecules. In Figure 5 and Table 4, the absolute values of the slope parameters for bands 1−4 are much larger than those for the other bands. Correspondingly, the negative peak shifts $\Delta E$ for bands 1−4 are also larger. However, the smaller negative slopes for bands 6−9 are accompanied by the positive $\Delta E$ values. According to their orbital characteristics shown in Figure 5, the repulsive interactions around the $CH_2$ and OH groups and along the CCl bond axis can be used to explain the smaller negative slopes and positive $\Delta E$ values for bands 6−9, whereas the larger negative slopes and negative $\Delta E$ values can be interpreted by the attractive interactions around the electron distribution regions of the $n_{Cl}$ and $n_O$ orbitals. In Figure 10a, the curves for the most attractive interactions exhibit the well depth to be ca. 80−90 meV. These values are close to the experimental $\Delta E$ for bands 2 and 3 ($\Delta E$ = −150 ± 60 and −150 ± 40 meV). The well depth in the curve for approaching to the O atom in Figure 10c is ca. 450 meV, which is close to the observed $\Delta E$ (−400 ± 100) for band 1 ($n_{O(Br)}$). In Figure 10c, the repulsive interactions for approaching the $CH_2$ group are consistent with the observations of smaller slopes of CEDPICS and positive $\Delta E$ values for bands 6−9. In Figure 6 and Table 5, the anisotropy of the

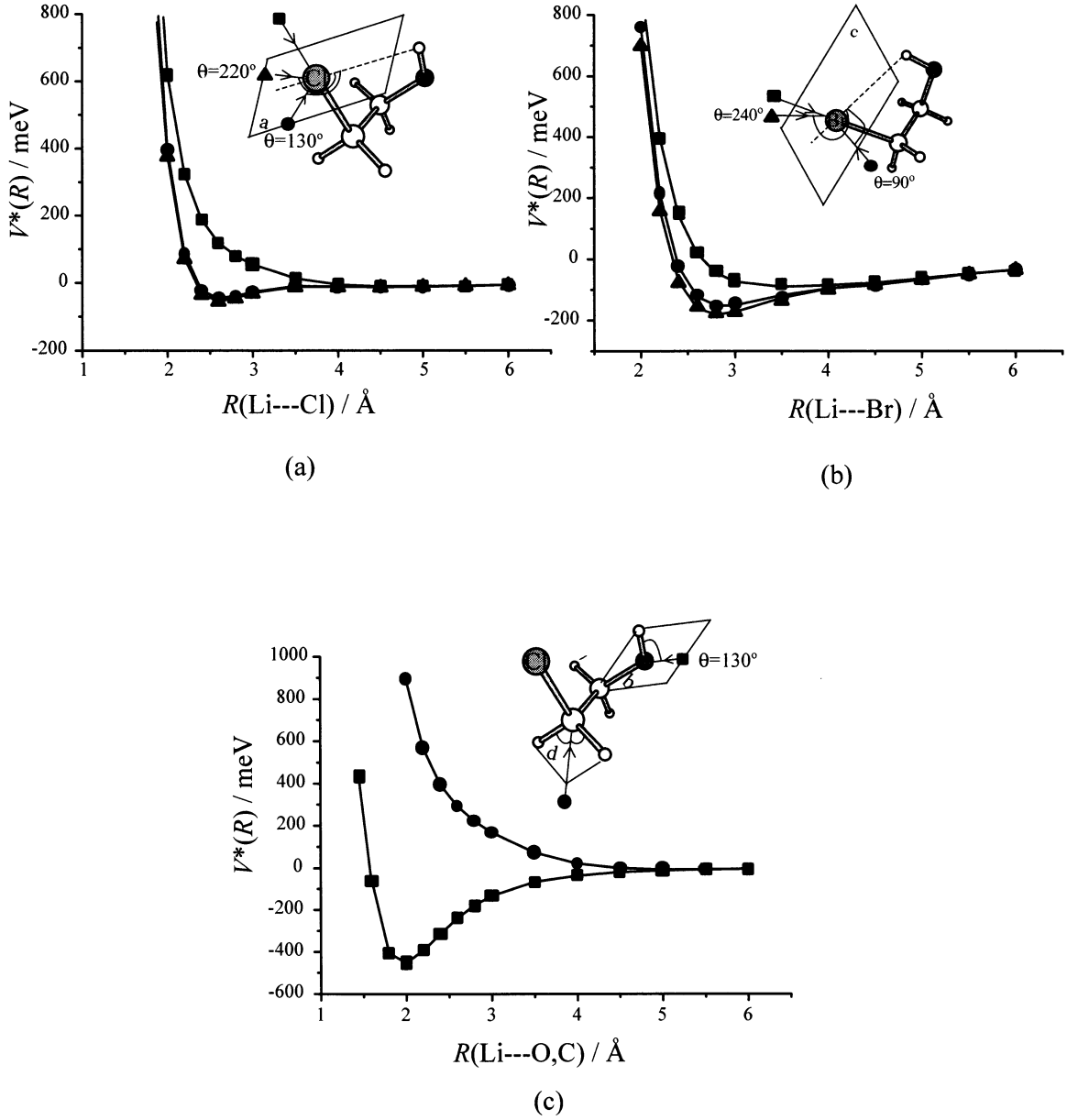


**Figure 10.** (a) Interaction potential energy curves $V^*(R)$ between Li and Cl. ■, the access along the C−Cl bond axis; ● and ▲, the approaches to the Cl atom at the $\theta \sim 130°$ and 220° at the plane a which is perpendicular to C−Cl bond axis. (b) Interaction potential energy curves $V^*(R)$ between Li and Br. ■, the access along the C−Br bond axis; ● and ▲, the approaches to the Cl atom at the $\theta \sim 90°$ and 240° at the plane *c* which is perpendicular to C−Br bond axis. (c) Interaction potential energy curves $V^*(R)$ between Li and O or C. ■, the access to the O atom at the $\theta \sim 130°$ at the plane *b* (the HOC plane); ●, the access to the C atom at bisector of the angle HCH at the HCH plane *d*. These $\theta$ values are the minima determined in Figure 9.

interactions around $BrCH_2CH_2OH$ is not as clear as around $ClCH_2CH_2OH$, because the He* trajectories are preferably approaching both the Br and O atoms. This steric effect leads to the averaged slope of CEDPICS for the outer valence bands for $BrCH_2CH_2OH$ are more negative than that for $ClCH_2CH_2$-OH. In Table 5, one can find that the negative slopes for bands 6−9 are smaller than those for bands 1−4, and the peak shifts for bands 6 and 7 are much smaller or even positive. It is noted that the largest negative slope and negative $\Delta E$ are observed for bands 4 and 5 due to the $n_O$ and $n_{Br}$ characteristics involved in the related orbitals (see Figure 6). The peak shifts for bands 1 and 2 ($\Delta E = -150 \pm 40$ and $-100 \pm 60$ meV) are close to the calculated potential well depth (140−170 meV) in Figure 10b.

Finally, we discussed the three lowest ionization potential bands for $ClCH_2CH_2OH$ and $BrCH_2CH_2OH$ on the basis of the CERPIES and CEDPICS measured at the high energy resolution condition. As shown in Figures 7a and 8a, the lowest intensity bands (band 1 for $ClCH_2CH_2OH$ and band 3 for $BrCH_2CH_2$-OH) are assigned as $n_{O(Cl)}$ and $n_{O(Br)}$, which is based not only on the band shapes as described by Ohno et al.[13] but also on the consistent analyses of CEDPICS and interactions given subsequently. In Figure 7b, band 1 shows the much flatter slope of CEDPICS than band 2 or band 3, in particular, the CEDPICS for band 1 even increases slightly with the increase of $E_c$ beyond ca. 200 meV. It can be interpreted by two effective approaches of attractive interactions (as represented by two big arrows pointing to $n_O$ and $n_{Cl}$ electron distribution regions) accompanied by two repulsive interactions (as represented by two broken curves) for the $CH_2$ and OH groups. The slightly increasing CEDPICS is arising from the repulsive interactions. Band 2 should show a larger negative slope of CEDPICS than shown

**TABLE 1: Relative Total Electron Energy without Correction of Zero Point Vibrational Energy ($\delta E_{tot}$, in kJ/mol) and with the Correction ($\delta E_{tot}^{ZPVE}$, in kJ/mol) and the Composition Ratios (%) for the Stable Isomers[a]**

| | gGX | | aGX[b] | | g′GX | | gAX | | sAX | |
|---|---|---|---|---|---|---|---|---|---|---|
| | | | | | X = Cl | | | | | |
| $\delta E_{tot}$ | 11.43 | 11.35 | 9.86 | 9.37 | 0.00 | 0.00 | 6.07 | 6.26 | 6.66 | 6.03 |
| $\delta E_{tot}^{ZPVE}$ | 10.59 | 10.46 | 8.53 | 7.76 | 0.00 | 0.00 | 5.60 | 5.64 | 5.50 | 4.47 |
| ratio | 1.1 | 1.1 | 2.5 | 3.3 | 79.5 | 75.5 | 8.3 | 7.7 | 8.6 | 12.4 |
| | | | | | X = Br | | | | | |
| $\delta E_{tot}$ | 12.99 | 13.14 | 11.48 | | 0.00 | 0.00 | 6.89 | 7.05 | 8.73 | 8.13 |
| $\delta E_{tot}^{ZPVE}$ | 11.74 | | 9.34 | | 0.00 | | 6.29 | | 7.19 | |
| ratio | 0.7 | | 2.0 | | 85.8 | | 6.8 | | 4.7 | |

[a] The data obtained at the DFT-B3LYP/6-31++G(d,p) and MP2/6-31++G(d,p) levels of theory are listed in the left and right columns, respectively. The ratios are estimated using eq 4. [b] The optimization of aGBr is converged to gGBr at the MP2 level of theory.

**TABLE 2: Geometrical Parameters (Bond Length in Ångstroms, Angles in Degrees) and Dipole Moment ($\mu$, in Debyes) of the Most Stable Conformer g′GX (X = Cl, Br) Using the 6-311++G(2d,2p) Basis Set**

| | DFT-B3LYP | MP2 |
|---|---|---|
| | g′GCl | |
| *r*(C1C2) | 1.514 | 1.511 |
| *r*(C1O) | 1.416 | 1.418 |
| *r*(C2Cl) | 1.825 | 1.804 |
| *r*(OH) | 0.963 | 0.962 |
| *r*(H···Cl) | 2.735 | 2.653 |
| *A*(C1C2Cl) | 110.74 | 110.01 |
| *A*(C1OH) | 108.20 | 107.19 |
| *A*(OHCl) | 108.67 | 110.58 |
| *D*(ClC2C1O) | 64.76 | 63.97 |
| *D*(HOC1C2) | −60.60 | −59.24 |
| *D*(HOC2Cl) | 2.260 | 2.558 |
| $\mu$ | 1.624 | 1.864 |
| | g′GBr | |
| r(C1C2) | 1.513 | 1.511 |
| *r*(C1O) | 1.415 | 1.418 |
| *r*(C2Br) | 1.990 | 1.954 |
| *r*(OH) | 0.964 | 0.962 |
| *r*(H···Br) | 2.821 | 2.743 |
| *A*(C1C2Br) | 110.94 | 110.47 |
| *A*(C1OH) | 108.22 | 107.28 |
| *A*(OHBr) | 111.31 | 112.80 |
| *D*(BrC2C1O) | 64.91 | 64.26 |
| *D*(HOC1C2) | −61.03 | −59.87 |
| *D*(HOC2Br) | 1.958 | 2.110 |
| $\mu$ | 1.640 | 1.864 |

in Figure 7b because of the serious overlap with band 1, which shows the flatter slopes. It is noted that the absolute value of the slope parameter for band 2 ($m = -0.43$) is a little larger than that for band 3 ($m = -0.41$), which can be interpreted by some composition of $n_O$ electrons in the orbital corresponding to band 2 whereas much fewer $n_O$ electrons in the orbital corresponding to band 3 (see Figure 7b). It is well-known that the $n_O$ orbital always corresponds to the strongly attractive interactions[7] (also see Figures 9 and 10c). Moreover, the slope for band 2 is slightly bended, which is exhibited by a broken curve in Figure 7b. This can be ascribed by a repulsive interaction around the OH group or the HB (H···Cl) region (see the second contour map in Figure 7b).

It is interesting to find the significant differences of CEDPICS for bands 1−3 between $ClCH_2CH_2OH$ and $BrCH_2CH_2OH$. For the $n_{O(Br)}$ band (band 3), the absolute value of its slope parameter ($m = -0.42$) is much larger than that for the $n_{O(Cl)}$ band. This is based on two facts: the compositions of $n_O$ electrons (ca. 80%) in the $n_{O(Br)}$ orbital are much larger than those (ca. 60%) in the $n_{O(Cl)}$ orbital;[33] the attractive interactions around the $n_{Br}$ electron distribution region are stronger than those around the $n_{Cl}$ electron distribution region. The slightly increasing (or the flatter) CEDPICS for band 3 is also observed in the higher $E_c$ region. To our surprise, the slope parameter for band 1 ($m = -0.46$) is much more negative than that for band 2 ($m = -0.38$). This should arise from their distinctly different MO electron distributions as shown in Figure 8b. There are no steric hindrances from the OH or $CH_2$ group for band 1, but there is

**TABLE 3: Energy Levels (−ϵ, eV) and Ionization Potentials Observed in UPS ($IP_{obsd}$ eV) and Those Predicted by the OVGF Calculations ($IP_{OVGF}$, eV) for g′GX, gAX, sAX, and aGX (X = Cl, Br)**

| | −ϵ | | | |
|---|---|---|---|---|
| | HF[a] | DFT-B3LYP[b] | $IP_{OVGF}$[c] | $IP_{obsd}$ |
| | | g′GX (X = Cl) | | |
| 1($n_{O(Cl)}$) | 12.88 | 8.03 | 11.55(0.92) | 10.68(10.91[d]) |
| 2($n_{Cl}$) | 12.01 | 8.49 | 10.99(0.92) | 11.27(11.48[d]) |
| 3($n_{Cl}$) | 12.16 | 8.70 | 11.25(0.92) | 11.50(11.71[d]) |
| | | g′GX (X = Br) | | |
| 1($n_{Br}$) | 11.17 | 7.88 | 10.62(0.92) | 10.52(10.62[d]) |
| 2($n_{Br}$) | 11.26 | 7.97 | 10.70(0.92) | 10.81(10.92[d]) |
| 3($n_{O(Br)}$) | 12.73 | 8.28 | 11.27(0.91) | 11.23(11.32[d]) |
| | | gAX (X = Cl) | | |
| 1($n_{Cl}$) | 11.87 | 8.35 | 10.84(0.92) | |
| 2($n_{Cl}$) | 12.00 | 8.73 | 11.09(0.92) | |
| 3($n_{O(Cl)}$) | 13.07 | 8.07 | 11.70(0.91) | |
| | | gAX (X = Br) | | |
| 1($n_{Br}$) | 11.10 | 7.78 | 10.51(0.92) | |
| 2($n_{Br}$) | 11.11 | 7.81 | 10.46(0.92) | |
| 3($n_{O(Br)}$) | 12.81 | 8.44 | 11.47(0.91) | |
| | | sAX (X = Cl) | | |
| 1($n_{Cl}$) | 11.94 | 8.30 | 11.01(0.92) | |
| 2($n_{Cl}$) | 12.00 | 8.37 | 11.03(0.92) | |
| 3($n_{O(Cl)}$) | 12.73 | 8.14 | 11.32(0.92) | |
| | | sAX (X = Br) | | |
| 1($n_{Br}$) | 11.00 | 7.75 | 10.44(0.92) | |
| 2($n_{Br}$) | 11.07 | 7.84 | 10.48(0.92) | |
| 3($n_{O(Br)}$) | 12.73 | 8.16 | 11.29(0.92) | |
| | | aGX (X = Cl) | | |
| 1($n_{Cl}$) | 11.74 | 8.20 | 10.74(0.92) | |
| 2($n_{Cl}$) | 11.83 | 8.51 | 10.92(0.92) | |
| 3($n_{O(Cl)}$) | 12.83 | 7.96 | 11.49(0.92) | |

[a] By the HF/6-311++G(2d,2p)//MP2/6-311++G(2d,2p) calculations. [b] By the DFT-B3LYP/6-311++G(2d,2p)//DFT-B3LYP/6-311++G(2d,2p) calculations. [c] By the OVGF/6-31+G(d)//MP2/6-311++G(2d,2p) calculations. [d] The values cited from ref 17.

**TABLE 4: Band Assignments, Ionization Potentials Predicted by the OVGF Calculations ($IP_{OVGF}$, eV) and Observed in UPS ($IP_{obsd}$, eV), Peak Shifts ($\Delta E$, meV), and Slope Parameters ($m$) for 2-Chloroethanol**

| band | orbital character[a] | $IP_{OVGF}$ (pole strength)[b] | $IP_{obsd}$ | $\Delta E$ | $m$ |
|---|---|---|---|---|---|
| 1 | $n_{O(Cl)}$ | 11.55 (0.92) | 10.68 | −400 ± 100 | −0.26[c] |
| 2 | $n_{Cl}$ | 10.99 (0.92) | 11.27 | −150 ± 60 | |
| 3 | $n_{Cl}$ | 11.25 (0.92) | 11.50 | −150 ± 40 | |
| 4 | $n_O$,$\sigma_{CCl,CH}$ | 12.79 (0.92) | 12.48 | −300 ± 80 | −0.33 |
| 5 | $\sigma_{CCl}$,$n_O$ | 13.84 (0.91) | 13.67 | −150 ± 100 | −0.18 |
| 6 | $\sigma_{CH,OH}$ | 14.83 (0.91) | 14.45 | 120 ± 100 | −0.18 |
| 7 | $\sigma_{CH}$ | 15.78 (0.92) | 15.60 | 60 ± 80 | −0.11 |
| 8 | $\sigma_{CH}$ | 16.46 (0.91) | 16.20 | 150 ± 80 | −0.15 |
| 9 | $\sigma_{OH,CH}$ | 17.95 (0.91) | 17.63 | 180 ± 60 | −0.09 |

[a] By the density maps in Figures 5 and 7. [b] The OVGF/6-31+G(d) performed over the MP2/6-311++G(2d,2p) optimized geometry of gG′Cl. [c] The parameters $m$ of bands 1−3 are −0.21, −0.43, and −0.41, respectively (see Figure 7b).

**TABLE 5: Band Assignments, Ionization Potentials Predicted by the OVGF Calculations ($IP_{OVGF}$, eV) and Observed in UPS ($IP_{obsd}$, eV), Peak Shifts ($\Delta E$, meV), and Slope Parameters ($m$) for 2-Bromoethanol**

| band | orbital character[a] | $IP_{OVGF}$ (pole strength)[b] | $IP_{obsd}$ | $\Delta E$ | $m$ |
|---|---|---|---|---|---|
| 1 | $n_{Br}$ | 10.62 (0.92) | 10.52 | $-150 \pm 40$ | $-0.39$[c] |
| 2 | $n_{Br}$ | 10.70 (0.92) | 10.81 | $-100 \pm 60$ | |
| 3 | $n_{O(Br)}$ | 11.27 (0.91) | 11.23 | $-180 \pm 40$ | $-0.42$ |
| 4 | $\sigma_{CH},n_{Br}$ | 12.52 (0.92) | 12.35 | $-400 \pm 80$ | $-0.45$ |
| 5 | $\sigma_{CBr},n_{O}$ | 13.36 (0.91) | 13.31 | $-200 \pm 80$ | |
| 6 | $\sigma_{CH,OH}$ | 14.67 (0.91) | 14.40 | $-60 \pm 80$ | $-0.24$ |
| 7 | $\sigma_{OH,CH}$ | 15.58 (0.91) | 15.45 | $10 \pm 100$ | $-0.21$ |
| 8 | $\sigma_{CH,CC},n_{O}$ | 16.28 (0.90) | 16.11 | $-300 \pm 100$ | $-0.29$ |
| 9 | $\sigma_{CH},n_{O}$ | 17.87 (0.91) | 17.62 | $-100 \pm 100$ | $-0.30$ |

[a] By the density maps in Figures 6 and 8. [b] The OVGF/6-31+G(d) performed over the MP2/6-311++G(2d,2p) geometry of *gG′Br*. [c] The parameters $m$ of bands 1−3 are −0.46, −0.38, and −0.42, respectively (see Figure 8b).

a strong hindrance due to the OH group (or the weakly HB (H···Br) region, because the overlapping densities between Br and OH are much fewer than those in the (H···Cl) region; see Figures 7b and 8b) for band 2. The latter is represented by an unequal label in the second contour map of Figure 8b. The similar steric shielding effects arising from the HB or OH group have been studied for the isomers of cyclohexanol.[7] It is also noted that the $n_O$ electron contributions to the first two orbitals of $BrCH_2CH_2OH$ are much smaller than those to the corresponding orbtials of $ClCH_2CH_2OH$. Furthermore, one may find that the spatial electron distributions of the lone pair $n_{Br}$ electrons differs from those of the $n_{Cl}$ electrons. This difference is also reflected by the calculated interaction curves in Figure 9. Two minima are found to be at ca. 130° and 220° for $ClCH_2CH_2OH$ whereas at ca. 90° and 240° for $BrCH_2CH_2OH$. In general, there are two factors leading to the different MO density distributions between $ClCH_2CH_2OH$ and $BrCH_2CH_2OH$: the HB in $ClCH_2CH_2OH$ is stronger than that in $BrCH_2CH_2OH$; the intramolecular $n_O \leftrightarrow n_{Cl}$ interaction is stronger than the $n_O \leftrightarrow n_{Br}$ interaction, which results in the mixed $n_{Cl}$ orbital having a little composition of the $n_O$ electrons. Both of them can be further reflected by the distinctly different CEDPICS.

## V. Concluding Remarks

Isomerism and intramolecular hydrogen bonding for $ClCH_2CH_2OH$ and $BrCH_2CH_2OH$ have been investigated with the DFT-B3LYP and MP2 calculations. The 2D-PIES including CERPIES and CEDPICS and He I UPS for these two molecules have been measured and analyzed on the basis of the calculations. Several conclusions can be derived: First, five stable isomers are found for each molecule, and the most stable one is the g′GX (X = Cl or Br) conformer, which is stabilized by the intramolecular hydrogen bonding. Second, the spectral assignments, particularly for the first three bands, are made on the basis of analyses their CEDPICS and calculated anisotropic interactions. The first band in the spectra of $ClCH_2CH_2OH$ is assigned as $n_{O(Cl)}$. The discrepancy of the lowest ionic state between the OVGF (and HF) predictions and experimental results is found for $ClCH_2CH_2OH$. Third, the steric hindrances (or shielding effects) by the hydrogen bonding and $CH_2$ groups are found in comparison of CEDPICS for bands 1−3. The magnitude of the hydrogen bonding in $ClCH_2CH_2OH$ is stronger that in $BrCH_2CH_2OH$, and the MO compositions of $ClCH_2CH_2OH$ differ from those of $BrCH_2CH_2OH$. These are closely related to the different CEDPICS for bands 1−3.

**Acknowledgment.** This work is partially supported by a Grant in Aid for Scientific Research from the Japanese Ministry of Education, Science and Culture. S.X.T. thanks the Japan Society for the Promotion of Science (JSPS) for a JSPS postdoctoral fellowship (ID No. 00111). Prof. J. V. Ortiz is acknowledged for the helpful discussion on the OVGF calculations for 2-chloroethanol.

## References and Notes

(1) Ohno, K.; Yamakado, H.; Ogawa, T.; Yamata, T. *J. Chem. Phys.* **1996**, *105*, 7536.
(2) Kishimoto, N.; Aizawa, J.; Yamakado, H.; Ohno, K. *J. Phys. Chem. A* **1997**, *101*, 5038.
(3) Kishimoto, N.; Furuhashi, M.; Ohno, K. *J. Electron Spectrosc. Relat. Phenom.* **1998**, *88*−*91*, 143.
(4) Yamazaki, M.; Kishimoto, N.; Kurita, M.; Ogawa, T.; Ohno, K.; Takeshita, K. *J. Electron Spectrosc. Relat. Phenom.* **2000**, *114*−*116*, 175.
(5) Yamauchi, M.; Yamakita, Y.; Yamakado, H.; Ohno, K. *J. Electron Spectrosc. Relat. Phenom.* **1998**, *88*−*91*, 155.
(6) Tian, S. X.; Kishimoto, N.; Ohno, K. *J. Phys. Chem. A* **2002**, *106*, 6541.
(7) Tian, S. X.; Kishimoto, N.; Ohno, K. *J. Electron Spectrosc. Relat. Phenom.* **2002**, *127*, 167.
(8) Hotop, H.; Niehaus A. *Z. Phys.* **1969**, *228*, 68.
(9) (a) Ohno, K.; Mutoh, H.; Harada, Y. *J. Am. Chem. Soc.* **1983**, *105*, 4555. (b) Ohno, K.; Harada, Y. In *Molecular Spectroscopy, Electronic Structure and Intramolecular Interactions*; Maksić, Z. B., Ed.; Springer-Verlag: Berlin, 1991.
(10) (a) Mitsuke, K.; Takami, T.; Ohno, K. *J. Chem. Phys.* **1989**, *91*, 1618. (b) Takami, T.; Mitsuke, K.; Ohno, K. *J. Chem. Phys.* **1991**, *95*, 918. (c) Takami, T.; Ohno, K. *J. Chem. Phys.* **1992**, *96*, 6523.
(11) Dunlavy, D. C.; Martin, D. W.; Siska, P. E. *J. Chem. Phys.* **1990**, *93*, 5347.
(12) Desiraja, G. R.; Steiner, T. *The Weak Hydrogen Bond in Structural Chemistry and Biology*; Oxford University Press: New York, 1999.
(13) Ohno, K.; Imai, K.; Harada, Y. *J. Am. Chem. Soc.* **1985**, *107*, 8078.
(14) (a) Becke, A. D. *J. Chem. Phys.* **1993**, *98*, 5648. (b) Lee, C.; Yang, W.; Parr, R. G. *Phys. Rev. B* **1988**, *37*, 785.
(15) Møller, C.; Plesset, M. S. *Phys. Rev.* **1934**, *46*, 618.
(16) Gardner, J. L.; Samson, J. A. R. *J. Electron Spectrosc. Relat. Phenom.* **1976**, *8*, 469.
(17) Kimura, K.; Katsumata, S.; Achiba, Y.; Yamazaki, T.; Iwata, S. *Handbook of He I Photoelectron Spectra of Fundamental Organic Molecules*; Japan Scientific: Tokyo, 1981 and references therein.
(18) Turner, D. W.; Baker, C.; Baker, A. D.; Brundle, C. R. *Molecular Photoelectron Spectroscopy*; Wiley: London, 1970.
(19) (a) Yee, D. S. C.; Stewart, W. B.; Mcdowell, C. A.; Brion, C. E. *J. Electron Spectrosc. Relat. Phenom.* **1975**, *7*, 93. (b) Hotop, H.; Hükler, G. *J. Electron Spectrosc. Relat. Phenom.* **1977**, *11*, 101.
(20) (a) Latajka, Z.; Bauteiler, Y.; Scheiner, *Chem. Phys. Lett.* **1995**, *234*, 159. (b) Dkhissi, A.; Alikhani, M. E.; Bouteiller, Y. *J. Mol. Struct.* **1997**, *416*, 1.
(21) Pauling, L. *The Nature of the Chemical Bond*; Cornell University: Ithaca, NY, 1960.
(22) (a) von Niessen, W.; Schirmer, J.; Cederbaum, L. S.; *Comput. Phys. Rep.* **1984**, *1*, 57. (b) Zakrzewski, V. G.; Ortiz, J. V. *Int. J. Quantum Chem. Symp.* **1994**, *28*, 23. (c) Zakrzewski, V. G.; Ortiz, J. V. *Int. J. Quantum Chem.* **1995**, *53*, 583.
(23) Ortiz, J. V.; Zakrzewski, V. G.; Dolgounitcheva, O. In *Conceptual Perspectives in Quantum Chemistry*; Calaist, J.-L., Kryachko, E., Eds.; Kluwer Academic: Dordrecth, The Netherlands, 1997.
(24) Rothe, E. W.; Neynaber, R. H.; Trujillo, S. M. *J. Chem. Phys.* **1965**, *42*, 3310.
(25) (a) Čermák, V. *J. Chem. Phys.* **1966**, *44*, 3781. (b) Hotop, H. *Radiat. Res.* **1974**, *59*, 379. (c) Illenberger, E.; Niehaus, A. *Z. Phys. B* **1975**, *20*, 33. (d) Haberland, H.; Lee, Y. T.; Siska, P. E. *Adv. Chem. Phys.* **1981**, *45*, 487. (e) Parr, T.; Parr, D. M. *J. Chem. Phys.* **1982**, *76*, 316.
(26) Hotop, H.; Roth, T. E.; Ruf, M.-W.; Yencha, A. J. *Theor. Chem. Acc.* **1998**, *100*, 36.
(27) Frisch, M. J.; Trucks, G. W.; Schlegel, H. B.; Scuseria, G. E.; Robb, M. A.; Cheeseman, J. R.; Zakrzewski, V. G.; Montgomery, J. A., Jr.; Stratmann, R. E.; Burant, J. C.; Dapprich, S.; Millam, J. M.; Daniels, A. D.; Kudin, K. N.; Strain, M. C.; Farkas, O.; Tomasi, J.; Barone, V.; Cossi, M.; Cammi, R.; Mennucci, B.; Pomelli, C.; Adamo, C.; Clifford, S.; Ochterski, J.; Petersson, G. A.; Ayala, P. Y.; Cui, Q.; Morokuma, K.; Malick, D. K.; Rabuck, A. D.; Raghavachari, K.; Foresman, J. B.; Cioslowski, J.; Ortiz, J. V.; Baboul, A. G.; Stefanov, B. B.; Liu, G.; Liashenko, A.; Piskorz, P.; Komaromi, I.; Gomperts, R.; Martin, R. L.; Fox, D. J.; Keith, T.; Al-Laham, M. A.; Peng, C. Y.; Nanayakkara, A.; Gonzalez, C.; Challacombe,

M.; Gill, P. M. W.; Johnson, B.; Chen, W.; Wong, M. W.; Andres, J. L.; Gonzalez, C.; Head-Gordon, M.; Replogle, E. S.; Pople, J. A. *GAUSSIAN 98*; Gaussian, Inc.: Pittsburgh, PA, 1998.

(28) Schaftenaar, G. *MOLDEN 3.4*; CAOS/CAMM Center: The Netherlands, 1998.

(29) Chitale, S. M.; Jose, C. I. *J. Chem. Soc., Faraday Trans. 1* **1986**, *82*, 663.

(30) (a) Kuhn, M.; Lutecke, W.; Mecke, R. *Z. Anal. Chem.* **1959**, *170*, 106. (b) Krueger, P. J.; Mettee, H. D. *Can. J. Chem.* **1964**, *42*, 327. (c) Mori, N.; Nakamura, E.; Tsuzuki, Y. *Bull. Chem. Soc. Jpn.* **1967**, *40*, 2189. (d) Buckley, H.; Giguère, D. A.; Daijiro, Y. *Can. J. Chem.* **1968**, *46*, 2917.

(31) Kolbjorn, H.; Hedberg, K. *J. Am. Chem. Soc.* **1973**, *95*, 8263.

(32) Pearson, R. G. *Inorg. Chem.* **1988**, *27*, 734.

(33) Mulliken atomic population analyses in the molecular orbitals (contribution of all atomic orbitals belonging to the same to the electronic density in a given molecular orbital) are performed at the HF/6-311++G(2d,2p) level. The percentages are normalized for each fully (doubly) occupied molecular orbital.